Optical Emission Enhancement of a Laser Induced Plasma with a Tuneable Optical Parametric Oscillator Pulsed Laser

by

Beau G. Greaves

A Thesis
Submitted to the Department of Physics
in Partial Fulfillment of the Requirements for
an Undergraduate Degree in Honours Physics [Medical Physics] with Thesis
at the University of Windsor

Windsor, Ontario, Canada

2017

Abstract

Research has been present in the field of laser-induced breakdown spectroscopy (LIBS) for over half of a century, but only in the past 10 years has this research moved forward in investigating potential methods of enhancements through targeting an atomic transition in the substance of interest, with either one or two laser beams. Over the past year in this lab, a system has been constructed and tested that allows for single and dual-pulse LIBS, with a tuneable laser. This allows for targeting on specific transitions, making measurements of potential enhancements due to increased scattering within the plasma possible. These measurements were initialized with a brief study on the effects of the single-pulse technique resonant laser ablation in a low intensity regime, and the dual-pulse technique resonance-enhanced LIBS (RELIBS), with a high intensity ablation laser.

Acknowledgements

I would like to thank previous students Russell Putnam, Anthony Piazza, and Vlora Riberdy for the work they did on neodymium and the initialization of construction on the dual pulse setup, that gave me the direction necessary for the completion of this project. Furthermore, I'd like to thank the lab group that I had the pleasure of working with, Paul Dubovan, Chris Heath, and Allie Paulick, for the tremendous help they have provided in the construction of the setup, processing of the data, and analyzing results, as I surely would not have been able to accomplish the goals laid out in this thesis if I did not have their support, both as work associates and friends.

Lastly and most importantly, I'd like to thank my advisor, Dr. Steven J. Rehse, for accepting me into his lab, providing me with valuable guidance and advice, and the countless hours he has spent educating me not only on theory, topics, and methods used in this lab, but the fields of physics and research as a whole. I was lucky to have such a thorough and caring advisor; this work would obviously not exist if not for him.

Table of Contents

List of Figures

List of Abbreviations

CCD: Charge-Coupled Device

DP-LIBS: Dual-Pulse Laser-Induced Breakdown Spectroscopy

ICCD: Intensified Charge-Coupled Device

IR: Infrared

LIBS: Laser-Induced Breakdown Spectroscopy

LIBS-LIF: Laser-Induced Breakdown Spectroscopy with Laser-Induced Fluorescence

LIP: Laser-Induced Plasma

LOD: Limit of Detection

MCP: Microchannel Plate

Nd:YAG: Neodymium-doped Yttrium Aluminum Garnet

OPO: Optical Parametric Oscillator

ppb: Parts per Billion

ppm: Parts per Million

RELIBS: Resonance-Enhanced Laser-Induced Breakdown Spectroscopy

RLA: Resonant Laser Ablation

SNR: Signal-to-Noise Ratio

UV: Ultraviolet

Chapter 1: Introduction

1.1: Motivation

Laser-Induced Breakdown Spectroscopy (LIBS) has been an actively researched method of atomic analysis since 1963[1], but in the past decade the methods of LIBS application have grown more complex in an attempt to decrease the limit of detection (LOD), while also decreasing the destructive impact of laser and plasma formation on the target. Of these applications, dual-pulse methods of LIBS appear to be one of the more promising techniques in the reduction of surface damage, but when this class of techniques is combined with a laser tuned to an atomic transition within the atom of interest, there is the potential to drastically decrease the LOD of a trace analyte within the target. A specific example of this is LIBS with laser-induced fluorescence (LIBS-LIF), a method where a plasma is generated via thermal mechanisms, and then using a low intensity laser with a wavelength tuned to a specific atomic transition to re-excite the plasma, one is able to see emission from only the energy level selected by the enhancement laser, allowing the LOD to decrease from the LIBS standard of parts per million (ppm) to parts per billion (ppb). Although this was not a method tested in this particular body of work, a large portion of the work done was the construction of a system capable of dual-pulse LIBS (DP-LIBS) with the ability to use resonant wavelengths to re-excite plasmas in both low intensity ($<10^8$ W/m^2) and high intensity ($>10^{12}$ W/m^2) regimes.

In this thesis, the work of previous students Russell Putnam[2] and Caleb Ryder[3] on neodymium was used to study resonant phenomena in this newly created LIBS system.

1.2: LIBS

In our laboratory, the focus of research is applications and enhancement of the spectrochemical technique of LIBS. In this analytic method, an ablative laser beam is focussed onto a target surface where it will ablate a small portion of material into a Laser-Induced Plasma (LIP). This plasma will contain highly excited atoms from the target being analyzed, and as these atoms de-excite they will release characteristic photons. The goal in LIBS is to collect these photons, disperse them within a spectrometer, and produce a time-resolved spectrum (graph of emission intensity as a function of wavelength) using a time gated camera. In the following section, the formation of plasma in the nanosecond regime will be discussed, while the method of light collection will be discussed further in Chapter 2.

1.2.1: Plasma formation

To produce a suitable measurement in a LIBS setup, the first task is to produce a high-temperature plasma capable of emitting enough characteristic photons, such that a suitable measurement can be attained. For a typical solid target, this will require a beam with an intensity of 10^8 - 10^{10} W/cm^2 with any wavelength, so long as it is suitably absorbed by the target material[4,5]. Given this threshold is met, a small portion of the target will be ablated, a process that can be seen in Figure 1.1 and described in detail in the paragraphs to follow.

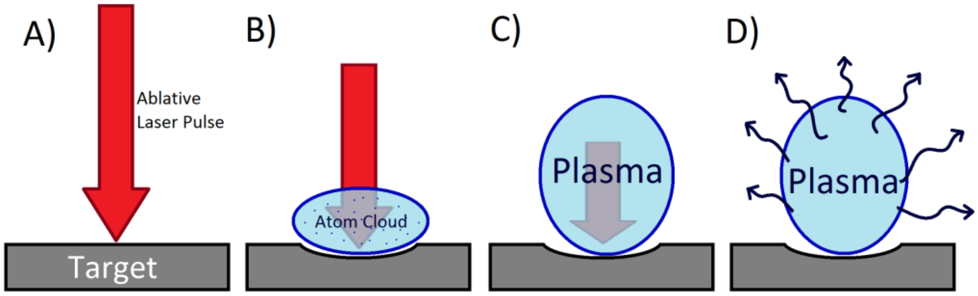

Figure 1.1: Formation of a laser-induced plasma, beginning with A) the impact of the ablative laser pulse, causing B) a cloud of atoms and microscopic debris to blast above the impact site where C) it will be ionized by the rest of the laser beam, forming an excited plasma that will D) emit characteristic photons that can be measured to determine internal composition of the target.

Each LIBS measurement is initiated by firing a focussed laser beam at a target, which initially blasts a cloud of both atoms and larger particulates of material above the impact site. Through inverse bremsstrahlung, a single photon interacts with an atomically bound electron to kick it out of its shell, resultantly ionizing the atom and generating a free electron, which will in turn cause a chain reaction within the atom cloud forming free electrons en masse, turning the cloud of material into an ionized plasma, from which higher energy states will arise through collisional excitations. At this point, the laser would still be in the process of impacting the target, but with the formation of the cloud of atoms above the laser impact site and generation of ions in said cloud, this newly formed plasma will begin to absorb the beam itself, causing it to flare out along the beam path of the laser, further exciting the plasma. Once the laser pulse ends, the expansion of the plasma will continue, but at a much lower rate, qualitatively shown in Figure 1.2 below.

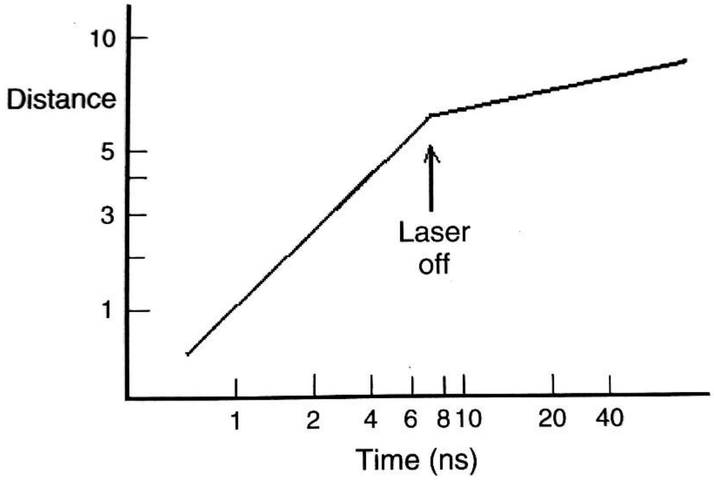

Figure 1.2: Relative displacement of the expanding luminous front of a plasma as a function of time[4].

From the time in which this plasma is excited, atoms within it will undergo de-excitations through both the release of characteristic photons and bremsstrahlung emission. The characteristic photons emitted will be dependent on the energy absorbed by the plasma, for ionized states will only commonly exist given a high enough temperature plasma, which can be seen in the Saha-Boltzmann equation (1):

$$N_e = \frac{I_0^*}{I_1^*} 6.04\text{x}10^{21} T^{2/3} e^{-\frac{E_{k,1}+E_{j,0}-E_\infty}{k_B T}} \tag{1}$$

Where N_e is electron density, $I^* = I\,\lambda/g\,A$ is a modified intensity of emission for two subsequent ionization states (denoted by the subscripts), T is temperature, E is the energy of the upper level at each ionization state (once again denoted by subscript), and E_∞ is the ionization energy for the lower ionization state.

Under the condition of a constant electron density, the temperature can be calculated through the ratios of emission from each ionization state, an example of which can be seen below in Figure 1.3, which consists of a graph produced by previous student Russell Putnam using atomic values for neodymium.

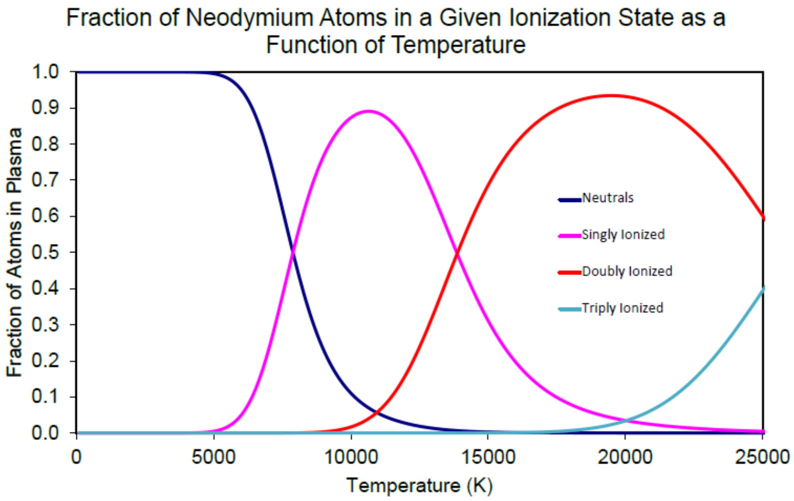

Figure 1.3: Graph of neodymium atoms at a given ionization state within a LIBS plasma as a function of temperature, generated by Russell Putnam[2], using the Saha-Boltzmann equation, neodymium atomic values, and an electron density of 10^{24} cm^{-3}.

The principles discussed in this section will later be applied when discussing the results of the experiments carried out, with a particular focus on ratios of ionization states.

1.2.2: Intro to RLA/DP-LIBS/RELIBS

Building off the central technique of standard LIBS analysis, the focus of the experiments carried out were to determine the potential benefits and functionally of three specific methods of LIBS application; those being resonant laser ablation (RLA), dual-pulse LIBS (DP-LIBS), and resonance-enhanced LIBS (RELIBS).

RLA builds off the standard model of LIBS by tuning the wavelength of the ablation laser to that of a known atomic transition of either the target atom or the matrix[6] (material in which the atom of interest is contained), or in other words, tuning the laser to a resonant wavelength. The transition for neodymium used for this experiment can be seen in Figure 1.4, with the allowed transitions for this energy level shown in the energy level diagram.

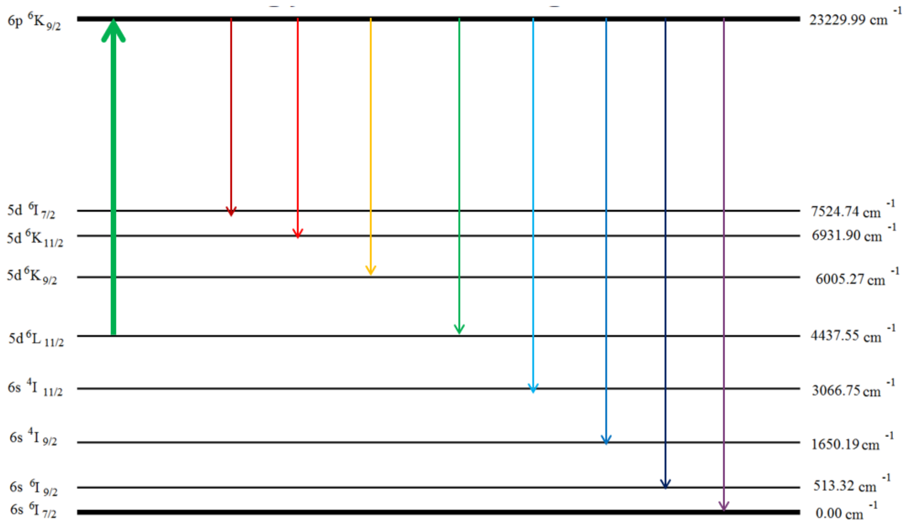

Figure 1.4: Energy levels in Nd II with the potential spontaneous emissions from the upper state shown on the right, while the resonant excitation wavelength used for the experiments in this paper, 531.982 nm, is shown on the left.

Contrary to RLA, DP-LIBS does not necessarily use any wavelength specific to the target material, but rather fires a second pulse after a known interpulse delay at the impact site of the first laser, re-exciting the plasma and causing an increase in emission. This technique proves to be particularly useful in cases where the target is ablated, but has poor plasma formation after the impact of the first laser.

The final technique combines the previous two techniques, and uses an off-resonance wavelength for the first ablative laser pulse, but follows this with a second, on-resonance laser pulse to enhance plasma emission. This method is of high interest to those researching non-destructive testing[6,7], but in the methods used by others the resonant wavelength of the second laser used is matched to a transition in the matrix, where in this case it will be directly matched to a transition in the target of interest, that being neodymium.

1.3: Scope of Thesis

The purpose of this thesis was to achieve the following goals.

The first goal was to build a functioning LIBS setup capable of both single-pulse LIBS with a 50 mJ pulsed 1064 nm Nd:YAG laser and dual-pulse LIBS setup using the 1064 nm Continuum laser and a 355 nm frequency-tripled Nd:YAG Quanta-Ray sent through an Optical Parametric Oscillator (OPO), allowing for the use of tunable wavelengths from 410 nm to 700 nm. The target was to be contained in a purge chamber capable of maintaining an argon environment at atmospheric pressure. A full description of the setup itself can be found in Chapter 2, with additional information on its construction found in Chapter 3.

The second goal was to measure the time dependant emission intensity of LIBS using only the beam produced by the OPO in two cases: with the beam wavelength matched to an atomic transition within the target (resonant laser ablation - RLA) and with the beam wavelength intentionally detuned slightly off that resonance wavelength. The on and off resonance cases will then be compared with the standard 1064 nm LIBS and with each other to determine relative emission intensity and temperature. This will be discussed in Chapter 4, Section 4.2.2.

The final goal in this thesis was to measure the time dependant emission intensity of DP-LIBS after the impact of the second laser pulse. There will once again be two cases analyzed, both will use the 50 mJ 1064 nm Nd:YAG as the main ablating laser (first pulse). The second laser will be generated from the 355 nm Nd:YAG and made tunable through the OPO such that the wavelength of the second beam is either: tuned to a transition within the target (RELIBS) or intentionally set to a length where the target has no transitions (DP-LIBS). Both cases were investigated with inter-pulse delays of 10 μs, 20 μs, and 25 μs. The time resolved intensity of each case at each inter-pulse delay will then be compared to each other and with the single-pulse 1064 nm LIBS to determine relative emission, enhancement, and temperature. Furthermore, the dual pulse emissions will then be qualitatively compared to the single pulse OPO LIBS and RELIBS cases, to see the differences in relative intensities, and temperature, using these differences to comment upon the possible significance of the method of excitation. This final topic will be discussed in detail in Chapter 4, Section 4.3.

1.4: References

[1] Radziemski, L. and Cremers, D. (2013). A brief history of laser-induced breakdown spectroscopy: From the concept of atoms to LIBS 2012. *Spectrochimica Acta Part B: Atomic Spectroscopy,87*, 3-10.

[2] Putnam, R. A. (2016). *Recent Advances in the Measurement of Rare-Earth Metal Transition Probabilities Using Laser-Induced Plasmas* (Master's thesis). University of Windsor.

[3] Ryder, C. A. (2012). *Oscillator Strength Measurements in Singly-Ionized, Doubly-Ionized and Neutral Lanthanides and Transition Elements (Sm, Nd, Pr, Gd, Cu, and Fe) Using Laser-Induced Breakdown* (Doctor of Philosophy thesis). Wayne State University.

[4] Singh, J. P., and Thakur, S. N. (Eds.). (2007). *Laser-induced breakdown spectroscopy*. Elsevier.

[5] Cremers, D. and Radziemski L., *Handbook of Laser-Induced Breakdown Spectroscopy*, 1st Ed. (West Sussex, England, 2006)

[6] Goueguel, C., Laville, S., Vidal, F., Sabsabi, M., and Chaker, M. (2010). Investigation of resonance-enhanced laser-induced breakdown spectroscopy for analysis of aluminium alloys. *Journal of Analytical Atomic Spectrometry, 25*(5), 635.

[7] Yip, W. and Cheung, N. (2009). Analysis of aluminum alloys by resonance-enhanced laser-induced breakdown spectroscopy: How the beam profile of the ablation laser and the energy of the dye laser affect analytical performance. *Spectrochimica Acta Part B: Atomic Spectroscopy, 64*(4), 315-322.

Chapter 2: Experimental Apparatus

From the very name of laser-induced breakdown spectroscopy, one could determine that the three fundamental components for this method of elemental analysis are a laser, spectrometer, and the target itself. For any modern study of LIBS applications or phenomena, these fundamentals need to be built upon with equipment to regulate the beam, target conditions, and plasma, as one could guess that simply firing the laser directly at target without any focussing optics would not be the most efficient method.

To that end, in the setup used for this set of experiments, the fundamental components were expanded to include two lasers: a 1064 nm Nd:YAG for ablation and a 355 nm frequency tripled Nd:YAG that is used to pump an optical parametric oscillator (OPO), producing an enhancement beam with a wavelength tuneable from 410 nm to 700 nm. The main ablation laser is controlled through software on the acquisition computer. With the addition of a second laser, complications arise with timing such that additional equipment is required to control when exactly it is fired. In this case, this necessitates a digital delay generator. Once fired, the two beams are run through an optical lens system to regulate the beam size and eventually focus each beam onto the target, which was contained in a sealed argon chamber to maximize plasma emission and reproducibility. A portion of this emission is captured by an optical fiber, which feeds the light into an échelle spectrometer that disperses it onto a time gated intensified camera, which through its corresponding software will generate an emission spectrum that can be viewed through the acquisition computer. A full schematic of the experimental setup can be seen in Figure 2.1.

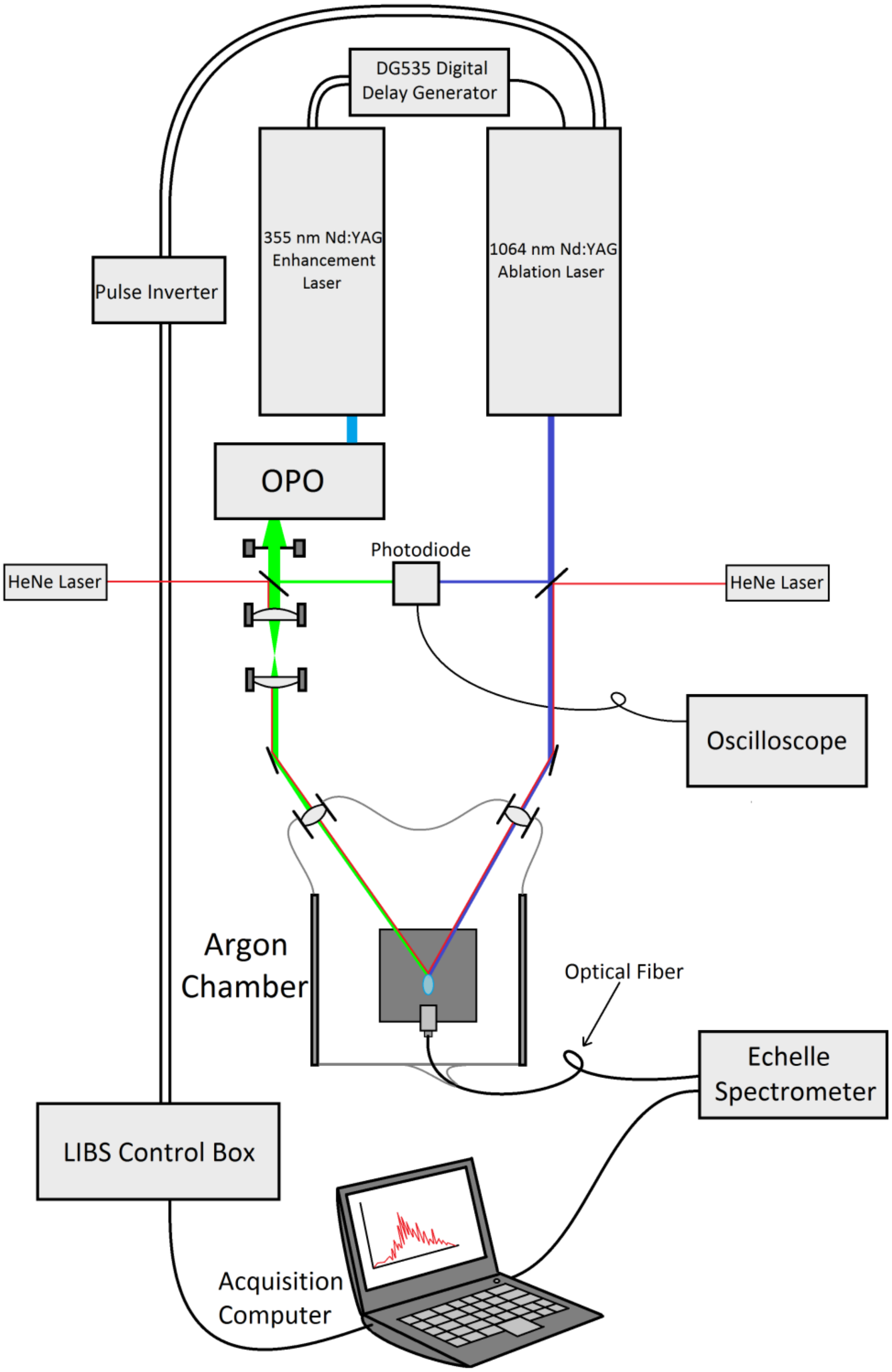

Figure 2.1: Full setup schematic, with the beams striking coincident to generate a plasma on the target within the argon chamber, which is viewed by the spectrometer using an optical fiber.

2.1: Lasers

As previously mentioned in the introduction to this chapter, two different lasers were used in this experiment, those being a Continuum Surelite I-10 1064 nm Nd:YAG pulsed laser used for the main ablation laser, and a Spectra-Physics Quanta-Ray Lab-150-10H 355 nm frequency-tripled Nd:YAG pulsed laser used for pumping the OPO. In the figure below, microscope images of the craters formed by each of these beams under different conditions are shown, and these images will be referenced throughout the next two subsections in regards to beam intensity calculations.

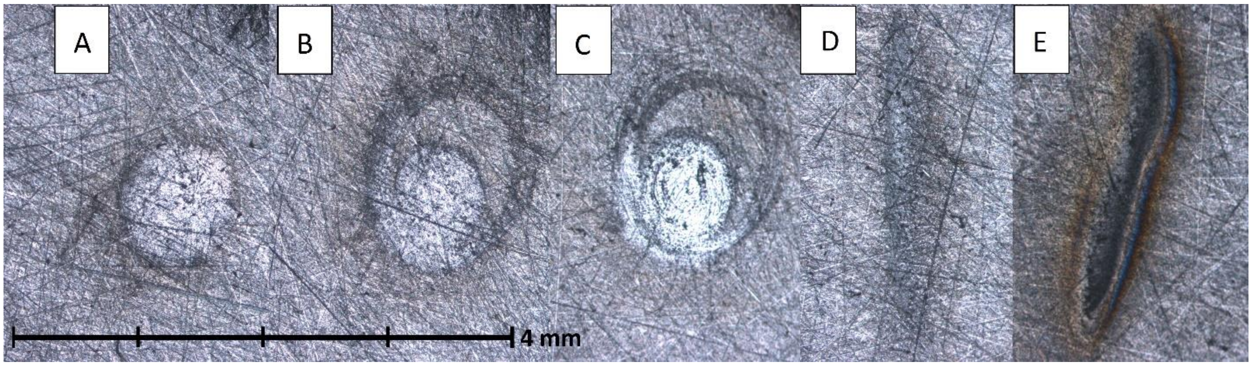

Figure 2.2: Crater images taken with a Leica Fluorescent Microscope with the help of Andrew Ouellette. The conditions for each crater were: A) single shot of the 1064 nm Nd:YAG in air, B) single shot of the 1064 nm Nd:YAG in argon, C) 10 shots operating at 10 Hz of the 1064 nm Nd:YAG operating in argon, D) approximately 1 shot of the 531.982 nm OPO beam operating in argon, E) approximately 20 shots operating at 10 Hz of the 531.982 nm OPO beam operating in argon.

2.1.1: Continuum 1064 nm Nd:YAG

In our lab, 1064 Nd:YAG lasers have a long history of being the workhorse for our LIBS setups, and this case is no different, as the source for high intensity ablation in this case was one of these very lasers. For this experiment, the 1064 nm Nd:YAG laser used is a Continuum Surelite I-10, which operates at 10 Hz and with a pulse width of 7 ns and pulse energy of approximately 150 mJ, which is lowered to 50 mJ upon impact onto the target. This beam was focussed onto the target using a 15 cm focal length spherical lens, producing an on-target spot size with a diameter of approximately 720 μm (measured using the average crater diameter in argon, seen in Figure 2.2B and 2.2C). Using this measurement and the beam properties mentioned earlier, this beam is found to have an on-target energy fluence of approximately 122000 J/m^2 and intensity of approximately 1.75x10^{13} W/m^2.

2.1.2: Spectra-Physics 355 nm Nd:YAG

To generate the tuneable laser wavelength, the OPO needs to be pumped by a high energy Ultra Violet (UV) source, which in this case is a Spectra-Physics Quanta-Ray 355 nm Nd:YAG, which is a standard Nd:YAG laser with the addition of a crystal at the output that generates third harmonic wavelengths from the 1064 nm beam, resulting in a high energy 355 nm beam. This laser operates at 10 Hz with a pulse width of approximately 9 ns and pulse energy of 200 mJ. When this beam pumps the OPO, the output energy decreases drastically and changes as a function of wavelength, with the highest beam energy occurring around 500 nm. At the wavelength used in the studies completed in this thesis, approximately 532 nm, the OPO beam had an pulse energy of 17.8 mJ upon entering the chamber, with altered dimensions to approximately 2.24 mm by 215 μm upon impact onto the target (measured using the OPO crater in Figure 2.2E). Using these measurements and the beam properties mentioned earlier, this beam is found to have an on-target energy fluence of approximately 37000 J/m^2 and intensity of approximately 4.1x10^{12} W/m^2.

2.2: Optical Parametric Oscillator

In order to produce the tuneable wavelength beam that was fundamental to this experiment, an ordinary pulsed laser could not be used. To produce this tunability in the wavelength of the beam, an Optical Parametric Oscillator (OPO) was installed and pumped by the 355 nm Nd:YAG. The OPO itself is a barium borate crystal on a rotational stage, with the fundamental principle behind its functionality being that if it is pumped with a high intensity 355 nm beam, non-linear effects will arise due to higher order terms in the polarization, splitting the beam into two different frequencies, a “signal” and “idler” beam, that sum to the frequency of the pump laser, as shown in the equation below:

$$\omega_{pump} = \omega_{signal} + \omega_{idler} \tag{2}$$

A picture of the setup can be seen in Figure 2.3 to allow for a better understanding of the geometry.

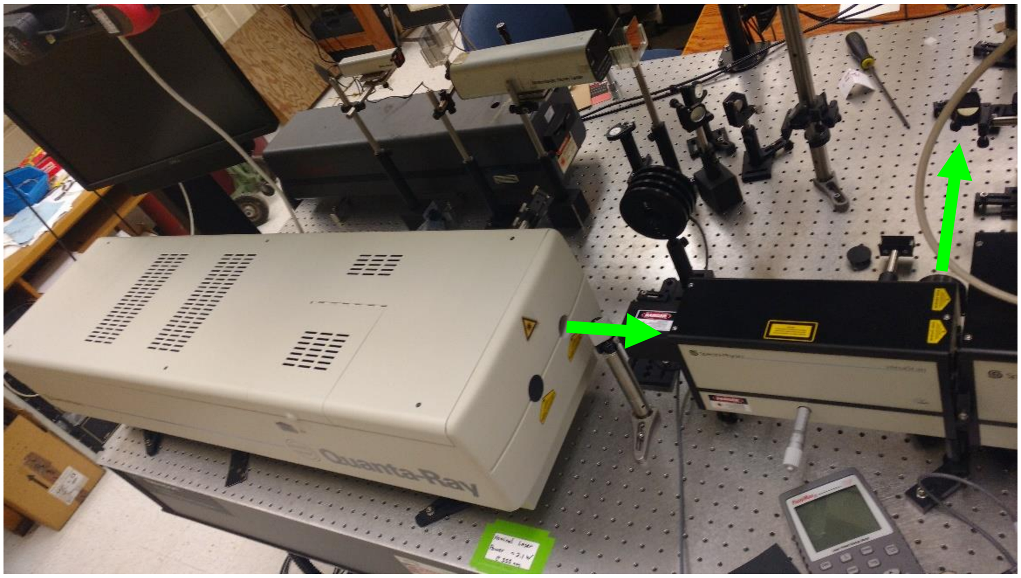

Figure 2.3: Picture of 355 nm Nd:YAG with arrows representative of laser light pumping the OPO, resulting in a signal beam, shown reflecting out of the OPO orthogonally.

As a brief proof of what is stated above, consider the following simple example from Hecht[1] of frequency mixing within a nonlinear dielectric. Let us begin with the following wave form:

$$E = E_{01} \sin \omega_1 t + E_{02} \sin \omega_2 t \tag{3}$$

If this wave form is substituted into the series expansion for the polarization, which is defined as:

$$P = \epsilon_0(\chi E + \chi_2 E^2 + \chi_3 E^3 + \cdots) \tag{4}$$

Then the resultant second order term will be:

$$\epsilon_0 \chi_2 (E_{01}^2 \sin^2 \omega_1 t + E_{02}^2 \sin^2 \omega_2 t + 2E_{01}E_{02}\, sin\, \omega_2 t\, sin\, \omega_2 t) \tag{5}$$

Where ϵ_0 is the permittivity of free space, E is the electric field, t is time, and χ is a unit less constant called the electric susceptibility. In the final equation, the first two terms can be represented as multiples of the first two wavelengths ($2\omega_1$ and $2\omega_2$ respectively), but the final term gives rise to sum and difference terms, $\omega_1 + \omega_2$ and $\omega_1 - \omega_2$, providing an example of the resultant signal and idler beam in this setup.

2.3: ARYELLE Échelle Spectrometer

To resolve the different wavelengths and intensities emitted from the plasma, the light is collected though an optical fiber that shines the light into an échelle spectrometer, in this case an ARYELLE 200 échelle spectrometer manufactured by Lasertechnik Berlin. This device will disperse the incoming light by sending it through a prism onto an échelle diffraction grating. With échelle having a French origin, translating to `ladder` in English, it is well suited to the grating itself, as the basis for the échelle grating`s function is its blazed, step-like, construction, as seen in Figure 2.4.

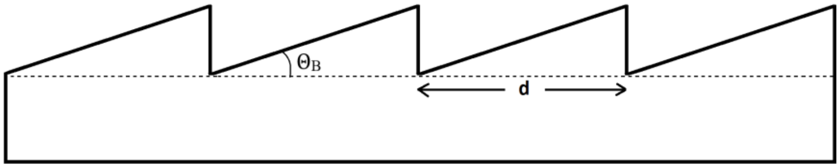

Figure 2.4: Basic geometry of an échelle grating, with θ_B equal to the blazing angle and d equal to the groove separation.

The function of this blazed construction is to disperse light into overlapping orders, such that angular spacing for a given wavelength decreases with an increase in diffraction order, as given by the échelle grating equation:

$$d[\sin(\theta_i + \theta_B) + \sin(\theta_m + \theta_B)] = m\lambda \tag{6}$$

where θ_i is the incidence angle of the light onto the grating and θ_m is the diffracted angle for a wavelength of the order m. Variables θ_B and d are physical parameters of the grating itself, respectively representing the blazing angle, which is the angle in which the steps are raised from the surface, and the groove spacing, which is the width of these steps. Both of these parameters can be better seen in Figure 2.4.

After having been diffracted on the échelle grating, the light will dispersed onto an intensified charge-coupled device (ICCD), which is a CCD preceded by a microchannel plate (MCP) image intensifier that allows a gain to be applied to the data during the acquisition process, increasing the overall intensity seen in the spectrum produced. This is done by the generation of photoelectrons (proportional to the to the intensity of the incoming light) when the light from the échelle grating hits the MCP, which can then be amplified by a gain voltage, before hitting a phosphor layer that produces a shower of approximately monochromatic photons, proportional to the number of photoelectrons, onto the CCD. Additional to the amplification, the voltage gain applied to the MCP also allows for nanosecond-resolved time gating, such that when it is applied there will be data measured, and when there is no voltage, nothing will be measured. The CCD is spatially resolved and will take the 2D diffraction pattern from the échelle grating (échellogram) and though the corresponding LTB Sophi software, a spectrum of intensity as a function of wavelength is created. A basic diagram of this process can be seen below in Figure 2.5.

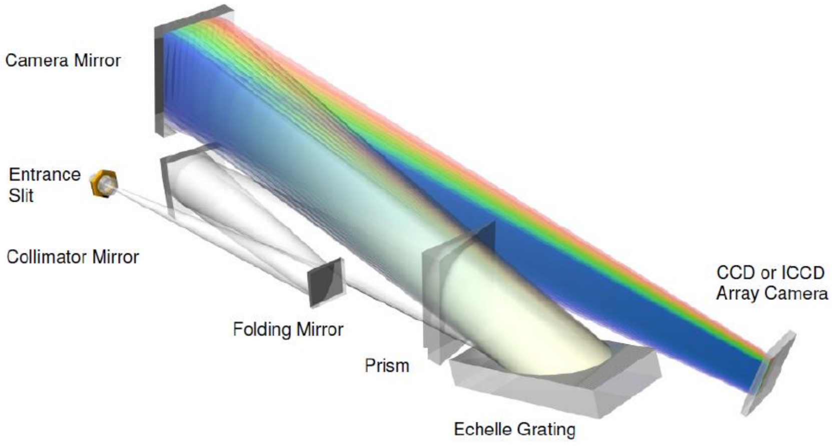

Figure 2.5: Diagram of the diffraction process in the ARYELLE 200 échelle spectrometer[2].

The result of this is that we are able to resolve a wide range of wavelengths, specifically from 200 nm to 800 nm, with a spectral resolution on the order of picometers and time resolution on the order of nanoseconds.

2.4: Timing Hardware

In the set of experiments completed, the main focus was probing the plasma with two laser pulses, but inconveniently for us, the software was only capable of triggering a single laser. To produce a dual-pulse laser setup, it was necessary that one laser be triggered off of the other, and for this to be possible, the following equipment was used.

2.4.1: Pulse Inverter

In the construction of this setup, some complications arose when attempting to first fire the 1064 nm Continuum as it only accepted negative TTL trigger pulses, whereas the spectrometer itself would only emit positive TTL pulses. To correct for this, a pulse inverter was constructed to take positive trigger pulses and output them as negative pulses in order to trigger the flash lamps and the Q-switch for the Continuum. The inverter consisted of two BNC inputs with two corresponding BNC outputs (one path for each of the flash lamp trigger and Q-switch trigger), and required an external power source in order to run.

2.4.2: DG 535 Delay Generator

In order to trigger the second laser (355 nm Nd:YAG), we required a system to produce both a delayed flash lamp trigger (at a controllable and known time after the trigger of the initial 1064 nm Nd:YAG) as well as a second pulse at an additional delay relative to the second flash lamp pulse to trigger the Q-switch of the 355 nm Nd:YAG. Both pulses are needed to cause it to fire, and both of these pulses had to have better than nanosecond control. To accomplish this task, a DG 535 delay generator was installed and triggered by the 1064 nm Continuum’s flash lamp sync output. In this way, the pulse to the 355 nm Nd:YAG was delayed a time defined as A=85.97 μs + (interpulse delay). If the interpulse delay is zero, the 1064 nm and OPO beams will be coincident in time on the target. A second pulse output was delayed a time defined as C=A+180 µs, and was used to trigger the Q-switch of the 355 nm Nd:YAG.

2.4.3: Photodiode and Oscilloscope

In order to know if the two laser pulses actually were coincident in time onto the target, a measurement system had to be put in place where both beams could be measured instantaneously and simultaneously. To do this, a photodiode was placed on the optical table such that scattered light from the widely diverging OPO beam would naturally be transmitted into it, and a beam splitter was used to take a small fraction of the 1064 nm beam and redirect it into the same photodiode. The photodiode was then connected to an oscilloscope that was triggered by the flash lamps of the 1064 nm Continuum laser, allowing one to see when the two pulses arrived at the photodiode in time relative to the triggering of the 1064 nm laser itself. An example of this can later be seen in section 3.4.

2.5: Argon Chamber

The argon chamber consists of a 4-faced polycarbonate cubic frame, with one face consisting of a magnetically-sealed door. This frame was set upon a 3D translation stage that has a 1 inch range of motion in both x, y, and z. Entering this chamber are three main parts: the laser beams, the optical fiber, and the argon input. The two lasers entered through their respective 15 cm converging lenses, while the optical fiber looked down onto the plasma at an angle of 50 degrees relative to the normal using another 3D translation stage that held the fiber, allowing for easy adjustments to be made to ensure as much light as possible was coupled into the fiber. The argon gas inlet tube was attached to the fiber holder for simplicity, as well as to minimize gaps that would be difficult to seal. A basic diagram of the chamber can be seen in Figure 2.6.

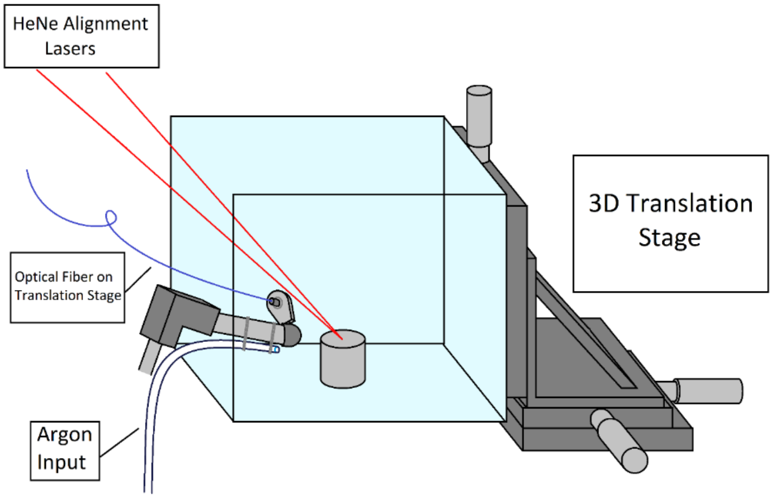

Figure 2.6: Basic diagram of the argon chamber construction, with the plastic shell sealing the apparatus not included in the diagram for simplicity.

The chamber was then sealed using a plastic membrane and adhesive, allowing for flexibility in its range of motion and the removal of all atmospheric gases from the chamber.

2.6: References

[1] Hecht, E. (2002). *Optics* (4th ed.). San Francisco, CA: Addison Wesley.

[2] Lasertechnik Berlin (2013). Manual ARYELLE – Spectrograph Series

Chapter 3: Setup Construction

Upon starting this project, I was not greeted with a blank table, but rather an initial system which allowed me to implement multiple ideas in how to move forward. The construction of this system was attributable to two previous students that had worked in the lab, Anthony Piazza and Vlora Riberdy. At this time, the two Nd:YAG lasers were in their permanent positions, with beam paths constructed for both the 1064 nm Nd:YAG Continuum and the 355 nm frequency tripled Nd:YAG Quanta-Ray (no beam path for the OPO). Although both beam paths were available, only the 355 nm Nd:YAG was capable of running off of the LTB software and there was no way of delivering a second pulse, making this setup exclusively capable of single-pulse LIBS. A helium-neon laser (HeNe) height finding system was in place at this time, using two 15 cm focal length lens placed such that the two visible HeNe beams converged when a target was at a height within the chamber measured to have the best-behaved emission. At this point, the chamber consisted of a box frame on a 3D translation stage, with an optical fiber looking down onto the impact location from the back side of the chamber. In this stage of construction there was also the addition of a USB camera which looked directly down onto the target that was used to ensure that a repeatable measurement could be made using the HeNe height finder. These components were then enclosed in a plastic film, which was the first attempt to create a sealed chamber, although at the time there was no method for argon input. Due to problems with translation flexibility and significant air leaks, the film attempting to seal the chamber had to be removed. As well, due to multiple issues in the reliability of the USB camera, it was also removed from the chamber I designed, although the implementation of a camera to ensure proper alignment is likely the next step forward in the design of the current chamber. A schematic of the LIBS setup at the starting point of this set of experiments can be seen below in Figure 3.1.

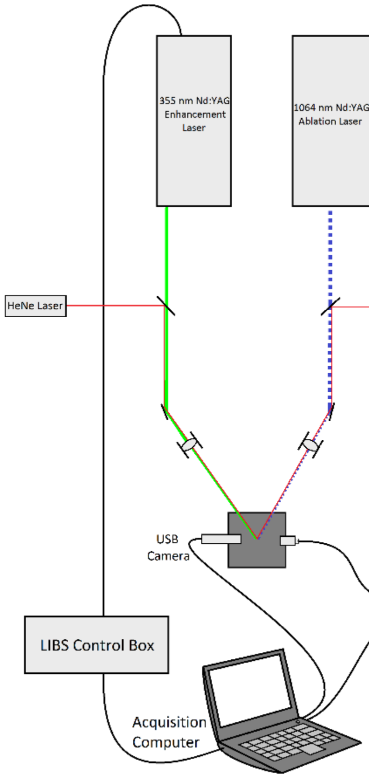

Figure 3.1: The setup construction at the beginning of my term in this lab, built by Anthony Piazza and Vlora Riberdy.

With this predefined starting point, there were several factors that needed to be considered when building the rest of the setup. The main goal in this LIBS setup was to build a beam path and timing sequence capable of dual pulse LIBS using the 355 nm pumped OPO and the 1064 nm Nd:YAG. In this beam path, it was required that the HeNe height alignment system stay in use, with each HeNe laser beam overlapping with an ablation laser beam at the impact location on the target for visualization. As well, the point in which the two ablation pulses met had to be contained in an adjustable chamber capable of being purged of air. Specifically, we needed to replace the air with another input gas at atmospheric pressure. The last requirement for the system was that there exist a way of controlling the pulse timing such that the time between the two ablation pulses could be measured, and that there exist a way to reliably measure each laser's operating power daily.

3.1: Beam Alignment and Height Finding

As mentioned previously, there were already some portions of the beam path constructed at the beginning of my term that had been built by previous students, which consisted of the 1064 nm path and the focussing optics into the argon chamber. The 1064 nm beam path consisted of two 1064 nm high reflecting mirrors set at 45° such that the beam was raised (for the purpose of chamber accessibility), parallel to its original position, and a 532/1064 nm dielectric mirror used to reflect the beam into the chamber at an incidence angle of 30°. The dielectric mirror was used for the final reflection of the beam for the singular purpose of keeping the 632.8 nm HeNe alignment beam overlaid with the ablation beam, as a 1064 nm mirror would not significantly reflect visible light. Inserting this mirror was not without consequence, as approximately 60% of the beam intensity is lost, but due to the high incoming pulse energy of the 1064 nm beam and the convenience of the height finding mechanism, this trade-off was acceptable.

The focussing optics for the chamber consisted of two spherical lenses with a focal length of 15 cm positioned such that both the 1064 nm Nd:YAG and 355 nm Nd:YAG were focused at a single point, with an angular separation of 40° between the two beams at impact, both hitting the target at a 35° angle of incidence. A visual of these impact angles is given in Figure 3.2.

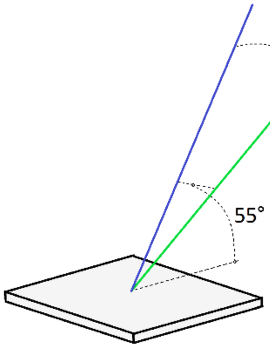

Figure 3.2: Geometry with which the two beams impact the target, with the 1064 nm Nd:YAG beam in blue and the OPO beam in green.

The first change made to the experimental setup was replacing the 355 nm beam path with an OPO beam path. As previously mentioned, the setup was capable of transmitting the 355 nm beam into the OPO at that time, but the OPO beam was not utilized within the setup. The output of the OPO is visible light with a wavelength in the range of 400 nm to 700 nm with a highly diverging elliptical beam. The first steps taken in controlling the beam were installing an iris (adjustable aperture) directly after the output of the OPO to minimize scattered light and eliminated portions of the beam with extreme divergence. After this step, the beam was reflected vertically with an aluminum mirror, then reflected horizontally towards the chamber with a 532/1064 nm dielectric mirror, once again for the purpose of chamber accessibility. The dielectric mirror was used in this case because it allows enough of the 632.8 nm HeNe beam to be transmitted such that there is still a working height finding system, while the majority of the intensity for OPO emission below 600 nm in wavelength was transmitted. To further minimize the beam divergence, a set of two cylindrical lenses with respective focal lengths 12.5 cm and 7.56 cm were placed in the beam path to create a cylindrical telescope, producing a smaller, more controlled spot size and a more collimated beam. This beam was then reflected into the chamber using another aluminum mirror, where it would overlap with the 1064 nm beam on the target after passing through the 15 cm focal length spherical lens. Below in Figure 3.3 is an overhead diagram of the beam paths as they are situated in the experimental setup.

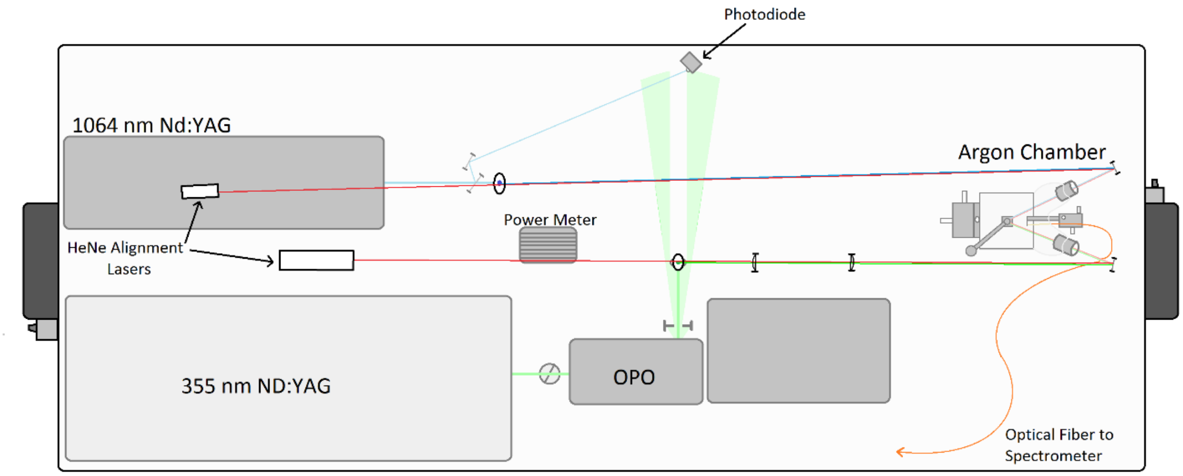

Figure 3.3: Overhead diagram of the beam paths and table setup.

3.2: Timing Scheme

With the two laser-pulse system, we required a sub-microsecond timing resolution with as little jitter in the pulse separation as possible.

In single-pulse LIBS, the pulse sequence is relatively simple. It is initiated with a positive flash lamp TTL trigger pulse being sent to the pulse inverter (where the pulse is inverted to negative, which can be used by the Continuum) from the LIBS box, a fast-pulse generator purchased from LTB with the spectrometer. The negative TTL pulse is then sent to the Continuum 1064 nm laser which fires the flashlamps which will create the population inversion of energy states in the Nd:YAG rod gain medium. After a 265 µs delay (set by the LTB Sophi software), a second pulse is sent from the LIBS box, triggering the Continuum Q-switch, causing the Nd:YAG rod to de-excite and fire the laser.

With the addition of the second laser, things quickly become more complex. Using the same pulse sequence for the Continuum as a beginning point, the addition of the second laser is built off of the flash lamp trigger sent to the 1064 nm laser at the beginning of the pulse sequence as the starting signal. An additional line is tee-d off of this pulse which triggers the DG 535 delay generator. The delay generator will then produce 2 pulses that are completely controllable in time and duration that will be used to fire the second enhancement laser. The first pulse is delayed a time A=85.97 µs + (interpulse delay) after the incoming trigger pulse, and this will cause the frequency-tripled 355 nm Nd:YAG Quanta-Ray laser to fire its flash lamps, causing a population inversion in its gain medium. The second pulse will be delayed a longer time of C=A+180 µs (or 265 µs specifically for coincident pulse impact), triggering the laser's Q-switch to fire, de-exciting the medium and sending out a 200 mJ pulse into the OPO, and then into the chamber itself. At this time, all that is left to do is measure the time-resolved emission from the plasma produced

3.3: Argon Chamber

Once the beam path had been constructed such that optics were fixed with the beams in focus and overlapping at the target position with a functioning height-finding mechanism, the final component required for its completion was the sealing of the chamber such that argon could be pumped in, displacing the air and maintaining an atmospheric or slightly over-pressure environment of argon.

To sustain this environment, the open parts of chamber containing both the converging lenses, the optical fiber, and the argon input were sealed with a shell composed of polymer film and adhesive, allowing for movement of the chamber without the misalignment of any of the focussing optics or interference with the beam. A study on how this chamber functioned can be seen in section 4.1.

3.4: Time Probing and Pulse Energy Measurement

As mentioned previously in both the introduction to this chapter and in section 2.4.3, in order to produce an accurate interpulse separation between the OPO and 1064 Nd:YAG, it was required to actually measure when the beams were incident in time with respect to each other. To do this, a photodiode was placed on the optical table in a location where the widely diverging OPO beam would naturally scatter a small amount of light into the device, and then a portion of the beam was split from the 1064 nm beam to redirect it into the photodiode as well. The geometry of this setup can be seen in Figure 3.3 at the beginning of this chapter. Sending the real-time data acquired by the photodiode to an oscilloscope and triggering said oscilloscope off of the 1064 nm Nd:YAG flash lamps, one was able to view the times in which the two beams hit the photodiode in respect to the when the first laser was initiated with sub-nanosecond resolution. An example image of the oscilloscope screen when a beam was present on the photodiode can be seen in Figure 3.4.

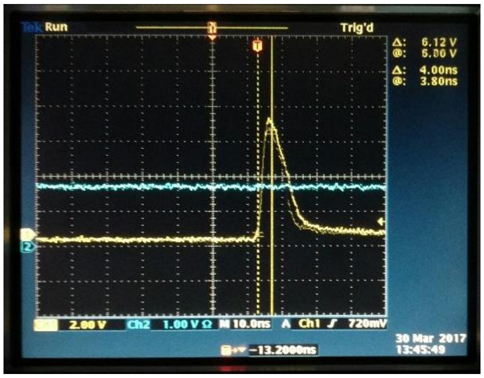

Figure 3.4: A picture taken of the oscilloscope display with the presence of the OPO beam tuned to 531.982 nm.

The next thing that was required to ensure that everything was working as expected was the installation of a pulse energy measurement system. When I began in the lab, half of this system was already in place, with a flip mirror present between the 355 nm Nd:YAG and the OPO, allowing one to put the mirror up and check the power output of the pumping laser. To make this functional for my setup, I had to measure the output of the OPO into the chamber for a constant 355 nm intensity and varying wavelengths of the signal beam, which in the end were used as factors multiplied onto the 355 nm pulse energy to determine the energy of an OPO pulse entering the chamber. To measure the pulse energy of the 1064 nm beam, a flip mirror was placed directly after the 1064 nm laser output, similarly to the 355 nm, and the beam was reflected into a power meter.

Chapter 4: Results

4.1: Argon Enhancement

With the beam path constructed and chamber sealed, the experimental setup was ready for measurements to be taken, the first of those measurements establishing the effect on plasma emission due to changes in the environmental conditions within the chamber caused by the addition of argon gas.

The baseline for this experiment was to repetitively fire the 1064 nm ablative laser at a steel target under atmospheric conditions, then, after a known amount of time, begin to pump argon gas into the sealed chamber and measure the effect on the plasma emission from the target and from the environment. Once a stable measurement was reached, the argon input was shut off and the chamber was left for an additional period of time, all while the laser continued to fire at the sample, giving insight into the stability of the chamber construction. Before ending measurements, the chamber door was opened to vent the contents of the chamber, and ideally to restore the chamber to its original conditions.

Stainless steel was chosen as the target for this experiment due to its non-reactive properties, wide availability, and regular usage within our lab group as a method of chamber calibration. In the alternate LIBS setup, data had previously been taken for the emission in air relative to the emission in argon, so this would allow for a quantitative comparison in the functionality of each chamber.

For this experiment, a 2.54 cm x 2.54 cm x 0.27 cm stainless steel plate was shot with the 1064 nm Nd:YAG in sets of ten 50 mJ pulses at 10 Hz every 2 seconds for a total of 550 seconds. After each set of pulses, the target was shifted such that the laser pulses were incident on a fresh piece of material, removing the variable of target degradation over time. Prior to taking measurements, the target was placed within the chamber, shutting the chamber door such that there was no gas entering or leaving the chamber. Measurements were then initiated, and at 100 seconds, argon gas was put into the chamber with a flow rate of 20 standard cubic feet per hour (SCFH) and the argon remained on and at this input flow until it was shut off at 300 seconds. After waiting an additional 200 seconds to determine the chamber's stability, the door was opened, purging the chamber of argon and returning it to its original state. Measurements were taken for an additional 50 seconds, after which the laser was shut off.

To analyze this data, atomic emissions of argon, oxygen, and iron were measured at 763.511 nm, 777.417 nm, and 358.119 nm respectively through peak integration, and the data found was used to produce the graph found Figure 4.1 below.

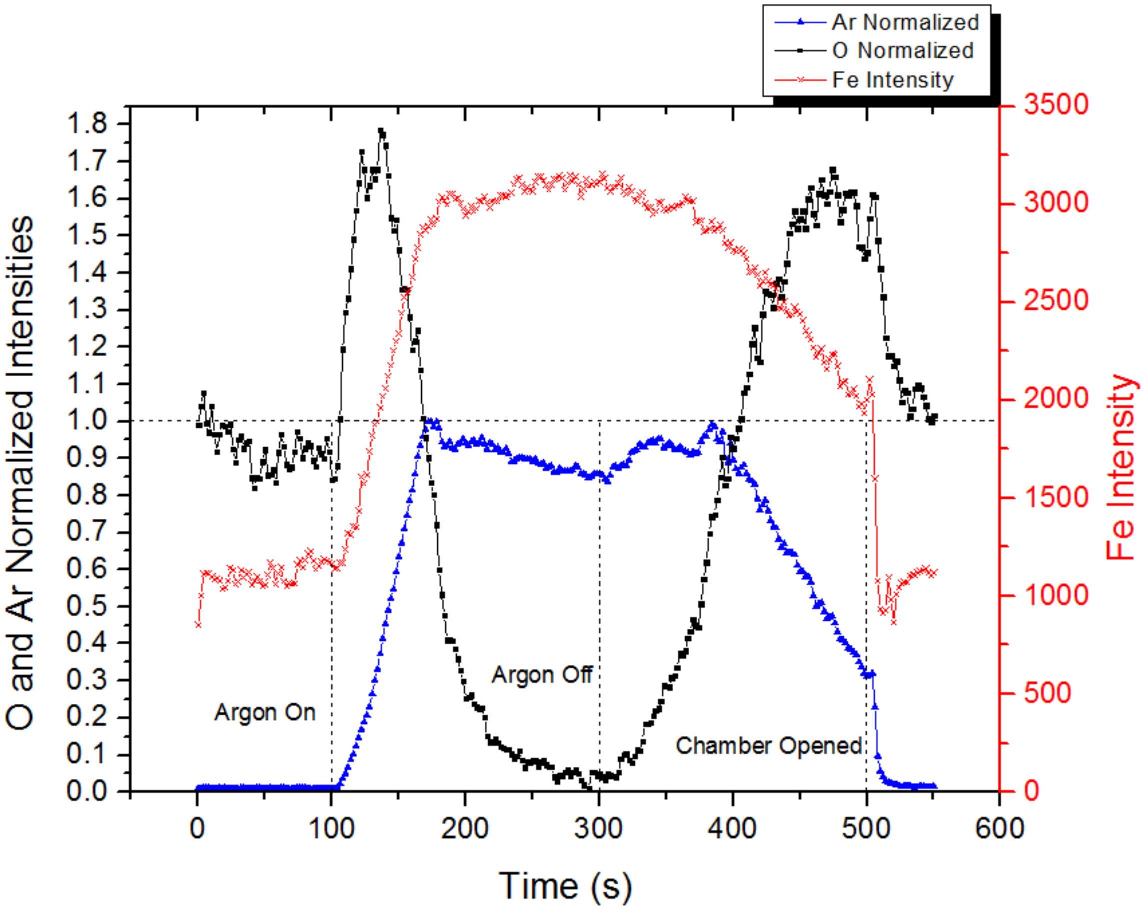

Figure 4.1: Graph of Fe 358.119 nm emission intensity, along with normalized O 777.417 nm and Ar 763.511 nm emission intensities as a function of the length of time that chamber was purged with argon.

In Figure 4.1, each point represents the integrated intensity from a single atomic emission line as a function of time relative to the start of the experiment. The emission intensities of argon and oxygen were scaled such that the intensity of oxygen was approximately 1 under atmospheric conditions and that the maximum emission intensity observed for argon was 1 as well.

The first motivation for this experiment was to determine if the chamber was functioning as expected, i.e. if it was capable of fully displacing the air from the chamber, filling it with only argon at atmospheric pressure. To determine if this was in fact the case with the chamber, the time resolved emission of argon and oxygen were analyzed using the data displayed in Figure 4.1. From time 0 to 100 seconds, the chamber contained only air, which establishes the initial condition for argon and oxygen emission, whereas oxygen intensity has been scaled to 1 in the graph and argon has zero emission, as it is not present. A close up of the two peaks of interest can be seen in the orange spectrum below in Figure 4.2.

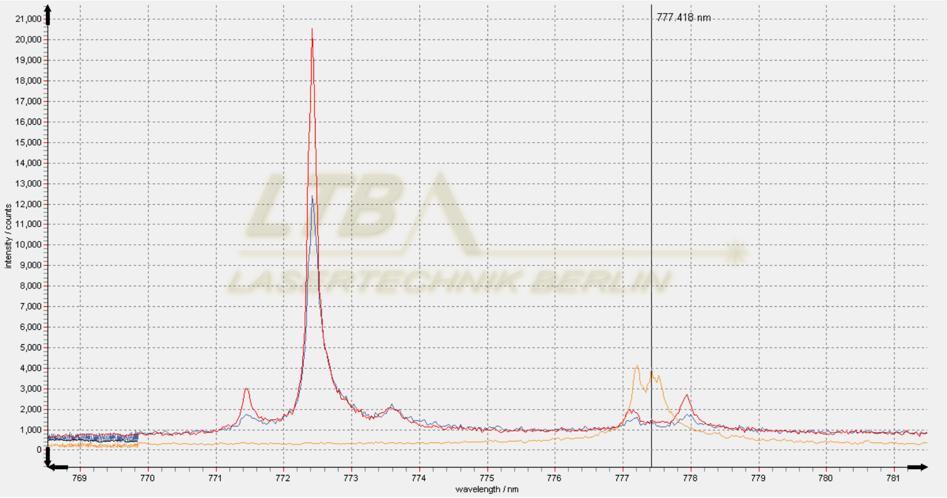

Figure 4.2: Shown above are 3 overlaid spectra displayed on the LTB Sophi software windowed such that the emission lines at 763.511 for argon and 777.417 nm for oxygen are shown. The orange spectrum was taken at 34 seconds (before argon had entered the chamber), the blue spectrum was taken at 272 seconds (once the chamber had been purged but the argon intensity was still increasing), and the red spectrum was taken at 300 seconds (when argon and iron emission had reached a stable measurement).

At 100 seconds, the argon valve was opened to 20 SCFH, causing argon to flow into the chamber and push out the gas previously contained within it. This can be seen in Figure 4.1

through the rapid increase of argon emission from 100 to 175 seconds. A detail that may be misleading in this case is that at the time that argon is sent into the chamber, the oxygen peak also increased drastically, nearly doubling from its original intensity for a short period of time before decaying to zero. This can be explained by the enhanced emission of a plasma in an argon environment, which will be touched upon in the following paragraph, but in short, the oxygen remaining in the chamber before being pushed out has enhanced emission intensity due to the interaction of argon with the plasma. As the argon pushes the oxygen out of the chamber, the emission from oxygen rapidly decays to zero (as can be seen in Figure 4.2 by the blue spectrum which was taken at 272 seconds into the measurement), but it also appears that the argon line is slowly decaying from approximately 170 seconds to when the argon is turned off at 300 seconds. This is indicative of the pressure increasing within the chamber, which would mean the flow of gas in is greater than that out. This means that the chamber is certainly sealed, but the current flow rate of argon is higher than ideal.

At approximately 220 seconds, it appears as though the plasmas from the steel target has reached a stable emission intensity, so the chamber was left to maintain this stable measurement for an additional 80 seconds before the argon flow was turned off at 300 seconds (the emission of the argon and oxygen at this time can once again be seen in Figure 4.2, in the red spectrum). As the argon input ended, the over-pressure was quickly released from the chamber with argon emitting more for this precise reason and the oxygen line quickly creeping up as it leaked into the chamber. At approximately 390 seconds enough argon had left the chamber to have a negative change in emission, all while the oxygen emission grew higher in the still-enhancing argon environment. At 500 seconds, the door to the chamber was opened quickly and all emissions returned to their original air values, as was expected.

The second goal in this experiment was to measure the enhancement in the emission from the target itself in an argon environment relative to ablation in air. This was done by analyzing the Fe 358.119 nm emission line plotted in red in Figure 4.1, with respect to time. Prior to argon being sent into the chamber, it can be seen that the iron emission is consistently hovering around a value of 1100 (arbitrary units), but immediately after the argon input was opened at 100 seconds the intensity rapidly increased, until approximately 170 seconds where there was a clear decrease in slope and the emission begins to plateau. Similarly to argon and oxygen mentioned in the previous paragraph, the iron emission seemed to grow consistent at 220 seconds, where it maintained an intensity around 3100 arbitrary units until the argon was once again shut off at 300 seconds, after which it eventually returned to its original value. This increase in intensity may seem odd to an outside perspective, but its use in LIBS systems has proven itself quite common because of its ability to drastically increase the signal-to-noise ratio (SNR). This increase in signal can be attributed to the lower transfer rate of energy from the plasma to the argon environment in respect to air. This is because the argon atoms are single unreactive noble-gas atoms that are relatively large relative to the atoms in air. As well, since it is a single atom, argon doesn't take on the vibrational states and spin states that would be present in a diatomic molecular gas, such as air (with N_2 and O_2), and because of this there is a lower rate of heat transfer that results in the plasma losing less energy over time. Generally, the more energetic and hotter the plasma is, the brighter it will be.

In conclusion, this experiment showed that the LIBS chamber that was constructed was capable of purging the environment of oxygen and maintaining these conditions under atmospheric pressure. From Figure 4.1, it can be interpreted that the chamber requires approximately 120 seconds of purging to reach a stable measurement with an argon flow rate of 20 SCFH, but would likely benefit from a lower flow rate as the increase in pressure has negative effects on the emission. Lastly, this experiment has shown that under the conditions of 10 shot sets operating at 10 Hz with individual pulse energies of 50 mJ and a measurement window (gate width) of 10 μs, an enhancement of approximately a factor of 3 can be expected for a steel target.

4.2: Single-Pulse LIBS on Neodymium

After having shown that the LIBS chamber was working as expected and having established conditions for ideal emission intensity, the next task was to take the first LIBS measurements. For the target in both single and dual pulse LIBS studies, neodymium was chosen due to its previous study in our lab, with investigations documenting the energy transitions and studying dual pulse resonant phenomena (LIBS-LIF) carried out by Caleb Ryder[1] and Russell Putnam[2] respectively. Although the measurements obtained in the single pulse LIBS experiments do not provide any new data in terms of what is known about Nd, it was required as it provided a suitable data set that could be used as a reference for following experiments. The neodymium target was 2.54 cm x 2.54 cm x 0.3 mm, and can be seen in Figure 4.3.

Figure 4.3: A camera picture of the neodymium platelet used as the target for both single and dual pulse LIBS experiments.

The goal in this experiment was to measure time resolved neodymium spectra with a constant gate width and increasing delay, such that the emission of the plasma could be characterized in respect to time. Three different wavelengths were used under two different power regimes.

4.2.1: 1064 nm LIBS on Nd

To accomplish the goal above, 31 spectra were acquired with increasing time delays from the moment of plasma formation. For each spectrum, the Continuum 1064 Nd:YAG was used to fire 10 pulses operating at 10 Hz with a 50 mJ pulse energy in an argon environment. Ten sets of shots (or 100 pulses) were averaged per spectrum. Each set of 10 shots was acquired on a fresh piece of target after target translation. The camera gate width (how long the camera observes the plasma) on each ablation was set to 10 µs and the gain was set to 1000 arbitrary units. In the context of this paper, the gain itself is not important as it is arbitrary in terms of its value, but the value used in this experiment was kept constant for those to follow to ensure that the intensity values measured had a meaningful relative value. A visual for how the measurements were taken can be seen below in Figure 4.4. With each spectrum, the only parameter varied was the gate delay, which is the timing between when the 1064 nm laser impacted the target and when the spectrometer looked at the plasma emission. Setting this gate delay to zero, the first spectrum was taken with a 0 µs gate delay, and with each additional spectrum the gate delay was increased by 1 µs, up to a maximum of 30 µs.

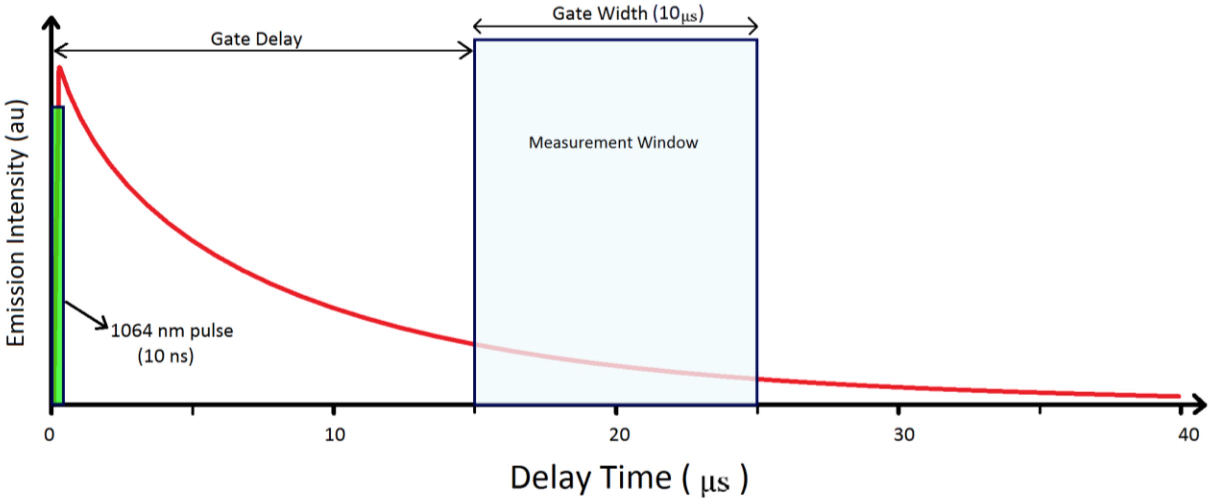

Figure 4.4: Diagram of time gating scheme used in the single-pulse LIBS experiments, with the expected decay of the plasma emission intensity shown in red.

After data acquisition had been completed, the next step was to process the data. Using the peak integration code described in Chapter 2 and located in Appendix B, 44 total emission lines were analyzed; 22 neutral lines (Nd I) and 22 ion lines (Nd II), the wavelengths of which can be found in Appendix A. A neodymium spectrum from this data set with a gate delay of 1 µs can be seen in Figure 4.5 below.

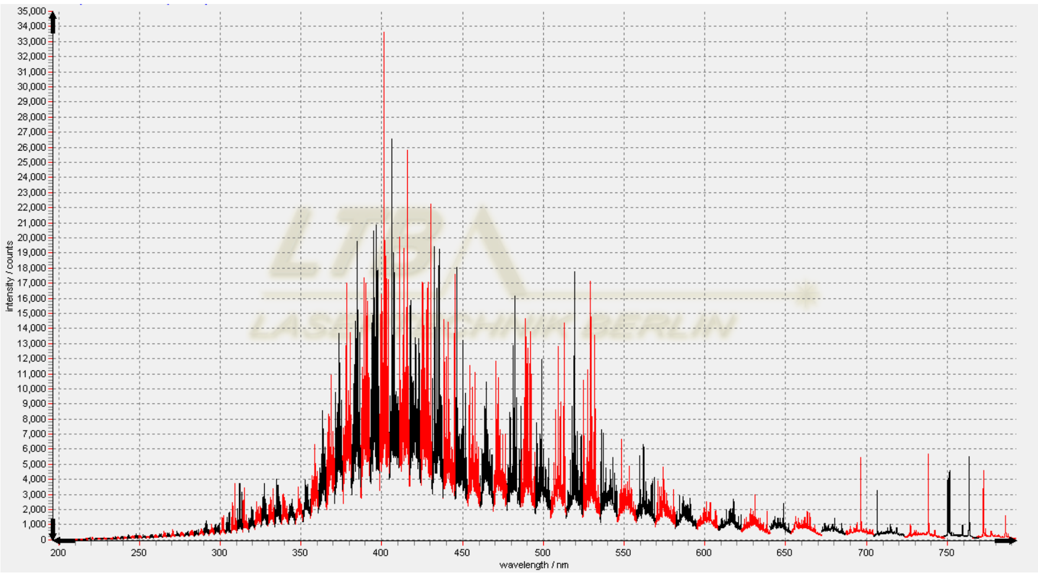

Figure 4.5: Neodymium spectrum taken using 1064 nm Nd:YAG at gate delay 1 μs.

Starting with the simplest case, to quantify the total time resolved emission, all 44 peak intensities were added at each gate delay, and after scaling the maximum total emission intensity measured to 10 au, the data were plotted as a function of the camera gate delay time. This data can be found in Figure 4.6 with both a linear and logarithmic scale, with the logarithmic scale to show the near exponential behaviour of the plasma emission decay.

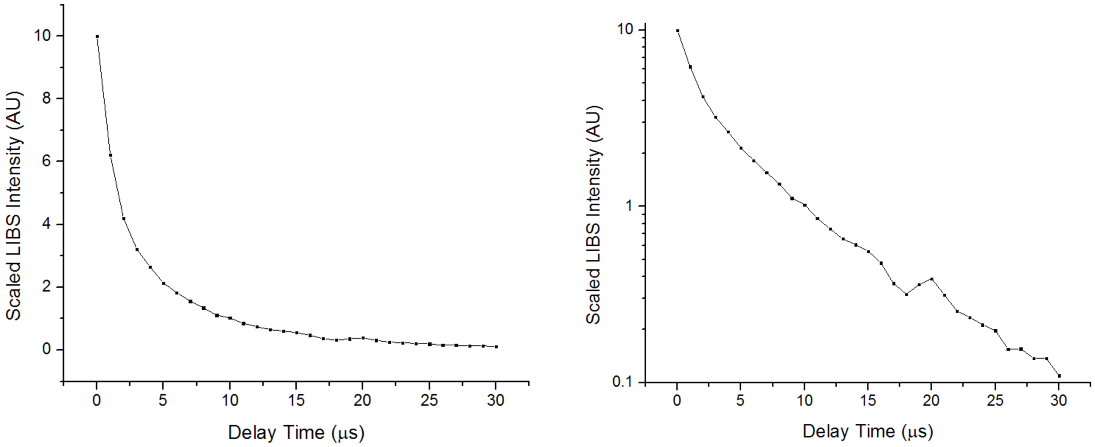

Figure 4.6: A scaled plot of the integrated emission intensity of Nd as a function of gate delay, using single pulse LIBS with the 1064 nm incident pulse, using the standard parameters introduced in the beginning of section 4.2.1.

4.2.2: OPO LIBS on Nd

Having measured the emission of neodymium using the well characterized method of high laser pulse energy LIBS with a 1064 Nd:YAG, steps could now be taken in a much less common direction, using the OPO to generate visible light for target ablation at wavelengths of interest. Taking advantage of the OPO's ability to tune the wavelength, this study was conducted on two separate wavelengths, 531.600 nm and 531.982 nm, where the second wavelength is exactly matched to an atomic transition between two Nd II energy levels that was previously studied by Russell Putnam in an investigation of LIBS-LIF[2]. The first of the two cases is considered to be no more than regular LIBS (albeit with a unique choice of ablation wavelength and much lower pulse energy), but to avoid confusion with the standard 1064 nm LIBS technique I have described earlier, from this point on ablation with the 531.600 nm beam will be referred to as OPO-LIBS. In the second case, having the wavelength of the OPO beam matched to the wavelength 531.982 nm, a transition wavelength in ionized neodymium, I will use a separate name due to the direct use of a resonant wavelength, this name being Resonant Laser Ablation (RLA). Due to the source of the beam, this technique will also subsequently be referred to as OPO-RLA within this thesis for clarity.

In taking measurements of the plasma emission with these two beams, the conditions were kept as close to the 1064 nm LIBS experiment as possible; leaving the camera gate width at 10 µs, operating frequency at 10 Hz, number of shots at 10, averaging sets of 10 shots, gain of 1000, and using the same measurement scheme as seen in Figure 4.4 (changing only the ablation beam). The only parameters that were forced to chance in this experiment were the pulse energy, which decreased to 17.8 mJ, and the on-target beam shape, which can be seen in Figure 2.2. Given these parameters and the measurement scheme used previously (taking 31 spectra with gate delays varying from 0 to 30 µs), the following graph was produced using the total emission intensity for the methods of OPO-RLA and OPO-LIBS

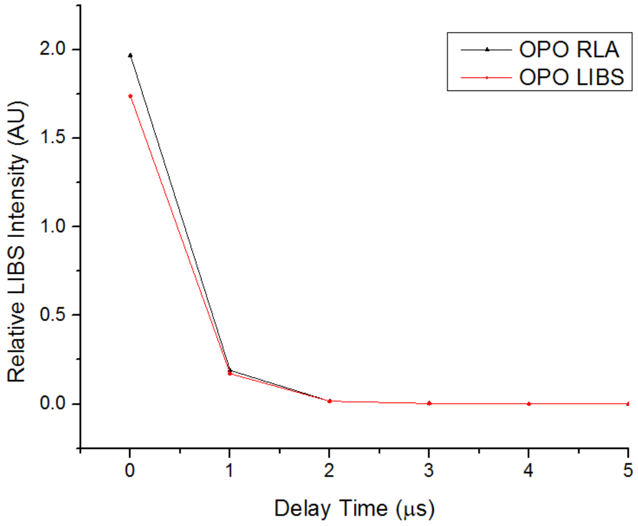

Figure 4.7: The integrated emission intensity of 44 Nd emission lines as a function of gate delay, using the single pulse methods of OPO-RLA and OPO-LIBS, using the standard parameters introduced in section 4.2.2. This graph is scaled to the maximum total emission intensity of the plasma formed by the 1064 nm Nd:YAG, shown in Figure 4.6.

The intensity and the rapid decay of the emission from both the OPO-RLA and OPO-LIBS cases indicates several things. The energy fluence has met the threshold for plasma formation and a spark has formed, but due to either the low on-target intensity or odd beam geometry, a robust plasma with significant atomic excitation is not achieved. This does not come as a surprise for multiple reasons, the first and most obvious being that both beams have a relatively low intensity compared to the 1064 nm laser and odd, elliptical beam shapes upon impact at the target.

To further compare the two OPO data sets with each other, the relative emissions due to each beam were analyzed by calculating the ratio of their emissions from their neutral and singly-ionized transitions. As well, the transitions originating from the upper energy level excited by the resonant pulse, shown in Figure 1.4 and denoted as 'Resonance' were analyzed.

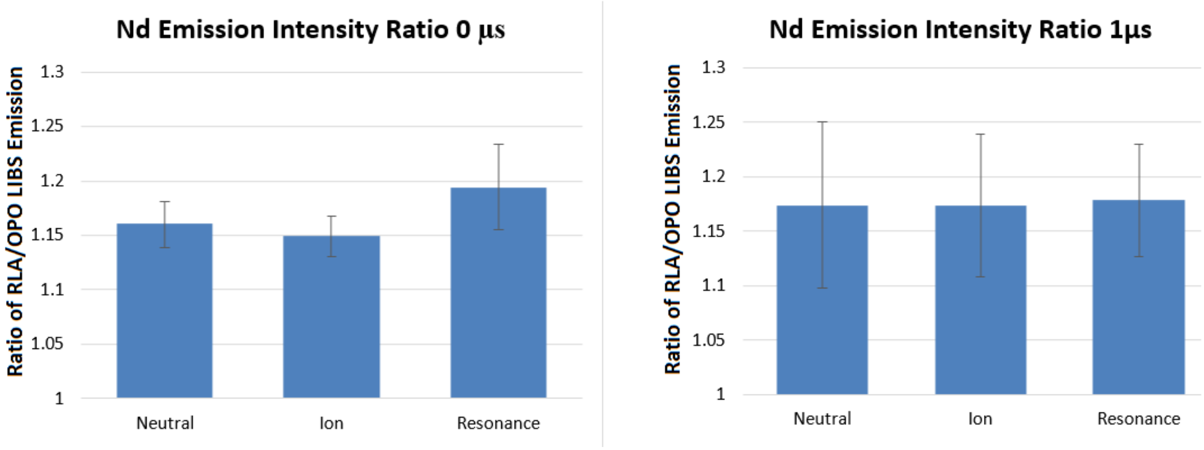

Figure 4.8: Ratio OPO-RLA/OPO-LIBS emission intensities from 3 different sets of transitions (neutral, singly ionized, resonance) at the gate delays of 0 µs and 1 µs.

Comparing the emission from the two single-pulse OPO methods in the graph above, it is clear that there is no notable difference in the emission ratio between any of the three categories of transitions, and if we refer back to the Saha-Boltzmann equation (1) in Chapter 1, the fact that there is no significant difference between the ratios in neutral emission and ion emission indicates that the two plasmas are approximately the same temperature, leading one to believe that the resonant beam alone has very little improvement relative to the non-resonance OPO-LIBS in the method's ability to form a hotter, more excited plasma. Once again, due to the low intensity and peculiar beam geometry, this would not come as a surprise. However, it can be seen in Figure 4.8 that there is in fact an apparent enhancement between the two methods of excitation, as the plasma emission intensity for the on-resonance case is approximately 1.15 times greater than that of the off-resonance case for both neutral and ion emission. Keeping true to our use of the Saha-

Boltzmann equation, this would suggest that since the ratios of ion to neutral emission is approximately equal between the two methods of excitation, the case of OPO RLA must give rise to a higher electron density, which in turn will give rise to a higher emission. A subtle detail in this experiment is that the resonant wavelength chosen is actually for a singly-ionized energy level, which in this case could suggest that since these states were not readily available, tuning the wavelength of the beam to this transition has no notable effect. For this reason, as well as the dissimilarities in expected plasma temperature relative to the actual emission ratios, a reasonable explanation for the enhancement phenomena present in this experiment has yet to be achieved, and further research on this topic will be required in the future.

4.3: Dual-Pulse LIBS on Neodymium

In the final study performed, the two lasers used independently in the experiments above were combined into a true dual-pulse experiment such that at some known interpulse delay after the 1064 nm Nd:YAG generated a plasma on the target surface, the target was then shot again, this time using the OPO beam. The emission measurements of the re-excited plasma were then taken at gate delays starting at 0 µs (after the OPO pulse), increasing in 1 µs increments until the measurement window was 30 µs after the initial production of the plasma (i.e. interpulse delay + gate delay = 30 µs). A basic timing scheme can be seen in Figure 4.9.

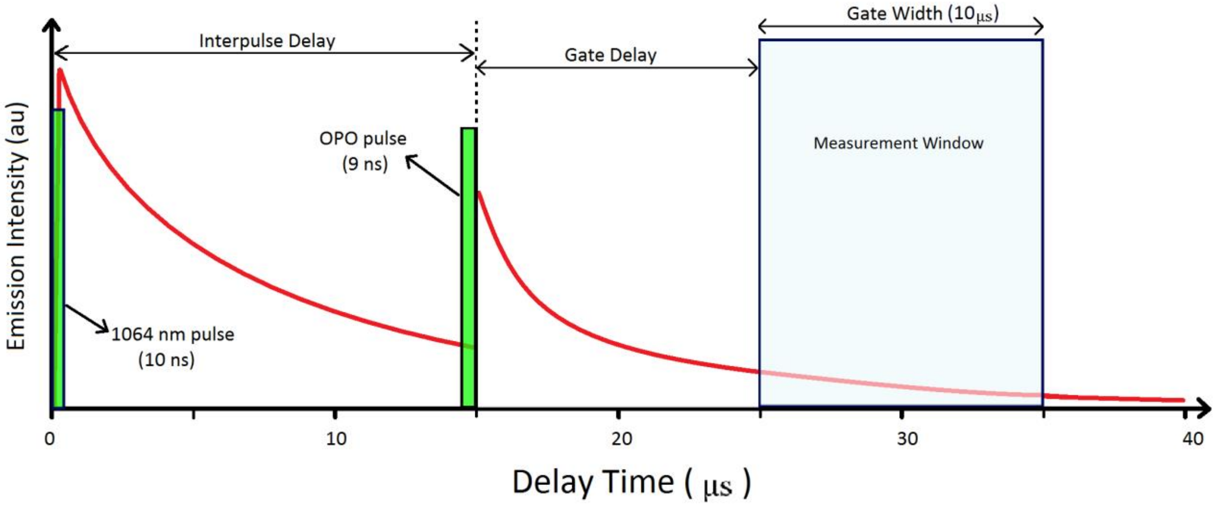

Figure 4.9: Diagram of time gating scheme used in the dual-pulse LIBS experiments, with the expected plasma emission intensity in red.

Maintaining the practice of using constant parameters, both the 1064 Nd:YAG and the OPO ran at an operating frequency of 10 Hz, with 10 shots from each averaged over 10 sets of shots, with an applied gain of 1000, and measurement gate widths of 10 μs. The two pulse energies were the same as in previous experiments, that is 50 mJ and 17.8 mJ for the 1064 nm Nd:YAG and OPO respectively. Continuing the emission measurements of resonant vs. non-resonant ablation, in this experiment the dual-pulse methods of RELIBS (on resonance) and DP-LIBS (off resonance) were investigated, with the respective wavelengths of 531.982 nm and 531.600 nm. The measurements taken with these imposed conditions and interpulse delays of 10 μs, 20 μs, and 25 μs are shown below in Figure 4.10, with the data from the single-pulse studies also shown for reference.

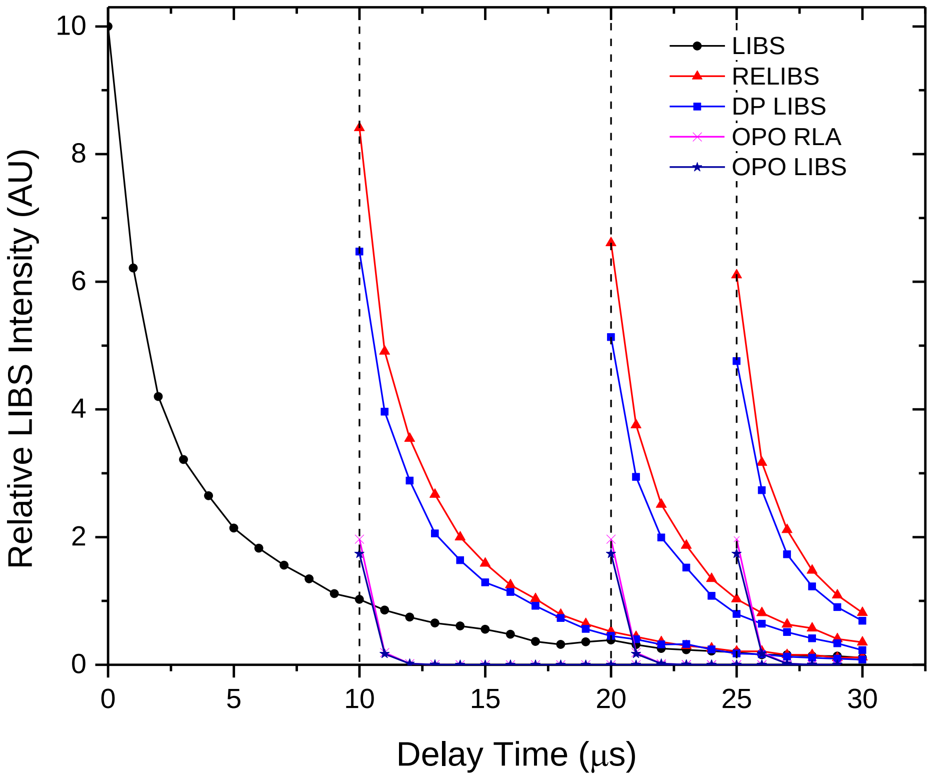

Figure 4.10: The integrated emission intensity of Nd as a function of gate delay, using the dual-pulse methods of RELIBS (red) and DP-LIBS (blue), using the standard parameters introduced in section 4.3. Overlaid in this graph are the emissions from the single pulse experiments done in section 4.2 for comparison (single pulse Nd:YAG LIBS in black, OPO-RLA and OPO-LIBS in magenta and navy respectively). All measurements are normalized to the same emission intensity scale.

The first thing that can be taken from this graph is the drastic change in plasma emission from RLA/OPO LIBS to RELIBS/DP-LIBS. Especially at the latter two interpulse delays when the emission from the plasma generated by the 1064 nm laser had nearly decayed to zero. There is a huge burst of emission upon the impact of the OPO beam that is far more significant than that of the plasma formed by the OPO beam alone. This indicates that the incoming OPO beam is no longer interacting with the target, but rather it is being intercepted by the plasma formed by the first 1064 nm Nd:YAG, which is much more receptive to the incoming photons in its already excited state. This also indicates that if a low emission plasma is formed initially due to poor conditions or a low intensity laser, if a second pulse were to re-excite the atom cloud it would likely be much more receptive to the incoming light, producing a significant enough emission intensity required for reproducible measurement.

The second thing to be noted from the previous graph is that a gap is arising between the emission of the RELIBS method and the DP-LIBS method. To further compare the two dual-pulse data sets with each other, the relative emission of each method was calculated as a ratio of their emission from their neutral and singly-ionized transitions, as well as the transitions originating from the upper energy level excited by the resonant pulse, shown in Figure 1.4 and denoted as 'Resonance'

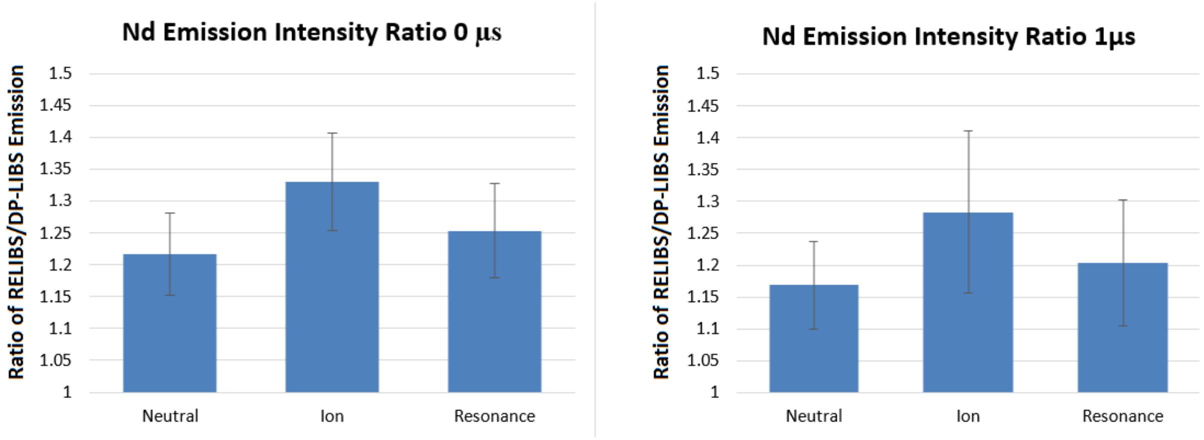

Figure 4.11: Ratio RELIBS/DP-LIBS emission intensities from 3 different sets of transitions (neutral, singly ionized, resonance) at the gate delays of 0 µs and 1 µs.

In the graph above, one feature that should immediately noted is the increase in emission ratios from the singly-ionized transitions relative to the neutral transitions. Making the necessary assumption of a constant election density between ablative methods used, we can refer back to the Saha-Boltzmann equation (1), which indicates that the enhancement plasma formed through RELIBS was hotter than the plasma formed by DP-LIBS, which in this case leads us to believe that tuning the laser wavelength to an atomic transition within the target does in fact cause the beam to couple into the plasma with a higher efficiency, resulting in a hotter plasma with more intense emission. Additional to this, the lack of enhancement of the resonant transitions that arise from decays out of the energy level that the OPO beam was tuned to excite indicates that the actual mechanism of enhancement is thermal in nature, rather than resonant. This supports the hypothesis that the increased emission in RELIBS relative to DP-LIBS is due to higher scattering of the resonant light within the plasma.

4.4: Preparation for Future Experiments on Neodymium

In preparation for studies regarding non-destructive testing using dual-pulse methods of LIBS, the final experiment done was to qualitatively determine the dependence of plasma emission intensity on the output power (or pulse energy) of the Nd:YAG laser. This was done by varying the operating voltage of the 1064 nm Continuum in increments of 0.2 V and taking a spectrum with 0 μs gate delay, 10 μs gate width, an accumulation of 10 shots per spectrum, and a gain of 1000. A graph of the data obtained can be seen below in Figure 4.12.

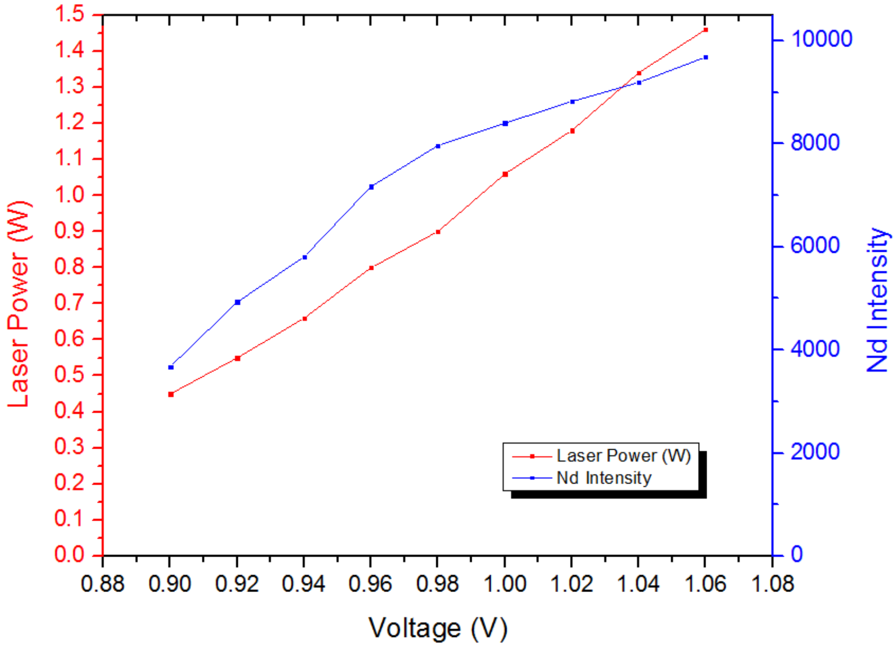

Figure 4.12: Measurement of plasma emission intensity and laser power as a function of the operating voltage of the 1064 nm Nd:YAG laser. The conditions for this measurement

were a gate width of 10 μs, gate delay of 0 μs, and an accumulation of 10 shots for each spectrum.

From this graph, it can be seen that at lower beam intensities, the plasma emission increases nearly linear with the laser power, but at the approximate halfway point in the operating voltage range, the plasma excitation begins to saturate, producing a lower than expected emission. This graph will hopefully give rise to a staring point on a study on the emission of DP-LIBS techniques as a function of initial-pulse energy.

4.5: References

[1] Ryder, C. A. (2012). *Oscillator Strength Measurements in Singly-Ionized, Doubly-Ionized and Neutral Lanthanides and Transition Elements (Sm, Nd, Pr, Gd, Cu, and Fe) Using Laser-Induced Breakdown* (Doctor of Philosophy thesis). Wayne State University.

[2] Putnam, R. A. (2016). *Recent Advances in the Measurement of Rare-Earth Metal Transition Probabilities Using Laser-Induced Plasmas* (Master's thesis). University of Windsor.

Chapter 5: Conclusion

5.1: Conclusion

Over the course of the past year, I have spent the majority of my time on this project constructing the setup itself, and this has resulted in a fully functioning LIBS setup capable of running LIBS, RLA, DP-LIBS, and RELIBS experiments under atmospheric pressures in an environment of argon. This experimental setup consists of two beam paths, one of which utilizes a tuneable OPO beam, that converge in a sealed argon chamber, where both beams are run by commands from a single computer, with one laser triggering off of the other.

With the successful construction of this setup, the methods of LIBS, RLA, DP-LIBS, and RELIBS were tested in this chamber using a neodymium target, 1064 nm high intensity ablation laser, and a tuneable enhancement laser using an off-resonance wavelength of 531.600 nm and on-resonance wavelength of 531.982 nm. From these experiments, evidence was found supporting the conclusion that low intensity beams are capable of generating significant plasma emission when the beam is incident on a previously produced plasma and that the mechanism of enhancement in RELIBS relative to DP-LIBS is increased scattering within the plasma leading to increased absorption efficiency of energy, due to the incident light being on-resonance with a transition in the plasma.

5.2: Future work

In regard to this experimental setup, the next step to be taken should be to optimize the functioning of the argon chamber, as the flow rate of argon was not kept at an ideal throughout the experiments done in this thesis. Also the installation of a visualization camera is required to develop an objective method of focussing the beams onto the target. From here, a significant step forward would be to develop a precise, experimentally-supported theory on why the on-resonance techniques produce a brighter plasma emission.

Continuing the work of RELIBS, an important next step would be to find its dependence on the wavelength of the excitation OPO laser and the energy of the laser pulses (both the ablation and enhancement pulses). Work in this area would hopefully lead to increase in the emission SNR, while reducing the destructive impact on the target material.

Once these dependencies have been found, work on non-destructive testing can begin in the lab, as well as measurements of trace-analytes using the techniques LIBS-LIF, which this experimental apparatus should be capable of running currently. Keeping with projects in our laboratory, a wonderful application of trace analyte detection would be on a project started by Vlora Riberdy[1] to characterize zinc deficiency in humans through the application of LIBS to fingernails, which she was capable of achieving, but with the setup she had at the time it was made tedious. Hopefully with the construction of this new, fully functioning setup, continuing projects such as these and starting new experiments will be made much more trivial.

5.3: References

[1] Riberdy, V. A., Frederickson, C. J., and Rehse, S. J. (2017). Determination of the Zinc Concentration in Human Fingernails Using Laser-Induced Breakdown Spectroscopy. *Applied Spectroscopy*, *71*(4), 567-582.

Appendices

Appendix A: Table of Nd wavelengths Investigated

Below is the list of the wavelengths used to characterize the emission of the neutral and singly ionized transitions in neodymium, as well as the 8 transitions that originated from the same energy level that was excited by the OPO in RLA and RELIBS, denoted by 'Resonance Emission Wavelength' in this Table.

Neodymium Transition Wavelengths used to Characterize the Plasma Emission Intensity		
Neutral (Nd I) Emission Wavelength (nm)	Ion (Nd II) Emission Wavelength (nm)	Resonance (Nd II) Emission Wavelength (nm)
455.967	388.078	430.357
456.322	390.021	440.083
460.987	391.116	463.424
462.194	395.115	495.814
463.424	397.327	531.982
464.640	401.225	580.402
468.345	406.108	613.358
469.644	407.512	636.729
471.902	410.945	-
477.946	413.533	-
494.483	415.608	-
495.478	420.559	-

506.373	432.577	-
529.167	438.566	-
541.173	440.083	-
572.929	444.639	-
574.919	445.157	-
582.674	482.548	-
588.791	513.059	-
600.767	529.317	-
628.579	527.343	-
631.049	562.054	-

Appendix B: Code for Peak Integration

The following code was written in the language Pascal by Chris Heath and Paul Dubovan in order to integrate the emission peaks from the LTB Sophi software such that an accurate, qualitative value could be found trivially.

```
Program test;
var
    line_num, i: integer;
    lamda, range, integral: double;
    line_info, spec_info, str_num: string;
begin
    (*intialize csv attribute*)
    DatabaseCSV.AddAttribute('Name');
    for i:=0 to 5 do
```

```
  begin
    if i < 10 then
      str_num:= '0' + IntToStr(i)
    else
       str_num:= IntToStr(i);
    spec_info:=
'C:\Paulsfolder\toanalyze\531dplibsbinaryongain1000gw10separation25delay_' +
str_num + '.esf';
    Spectrum.Load(spec_info);
    line_num:= 3;
    FileHandling.FileOpen('C:\Paulsfolder\sophi_config8.txt');
    (*DEBUG*)
    (*UI.ShowMessage(spec_info);*)
    (*excell formatting*)
   DatabaseCSV.AddValueAsString('Name', 'Integral' + IntToStr(i));
    while FileHandling.FileReadLn(line_num, line_info) do          (*continues as
long as there exists a line at index line_num*)
    begin
       lamda:= StrToFloat(Copy(line_info, length(line_info) - 13, 8));    (*Copy specific
number of characters off the end of the line*)
       range:= StrToFloat(Copy(line_info, length(line_info) - 4, 4));
       Delete(line_info, length(line_info) - 13, 14)              (*Deletes numbers at
end of line leaving the beggining id*)
       if i = 0 then
         DatabaseCSV.AddAttribute(line_info);
      (*look into how intensity and integral are being calculated internally*)
```

```
            integral:= Spectrum.GetIntegral(lamda - range, lamda + range);
               (*adds intensity and integral under elmt attribute*)
            DatabaseCSV.AddValueAsFloat(line_info, integral);
            line_num:= line_num + 1;
            end;
            FileHandling.FileClose;
    end;
    DatabaseCSV.ExportFile('C:\Paulsfolder\IntegralTest.csv');
    DatabaseCSV.DeleteTable;
end.
```